Journal of Power Sources 254 (2014) 249–257

Contents lists available at ScienceDirect

Journal of Power Sources

journal homepage: www.elsevier.com/locate/jpowsour

In situ growth of $NiCo_2S_4$ nanotube arrays on Ni foam for supercapacitors: Maximizing utilization efficiency at high mass loading to achieve ultrahigh areal pseudocapacitance

Haichao Chen, Jianjun Jiang*, Li Zhang, Dandan Xia, Yuandong Zhao, Danqing Guo, Tong Qi, Houzhao Wan

School of Optical and Electronic Information, Huazhong University of Science and Technology (HUST), Wuhan 430074, China

HIGHLIGHTS

- $NiCo_2S_4$ nanotube arrays have been synthesized based on the anion-exchange reaction.
- The specific structure achieves high utilization efficiency of $NiCo_2S_4$ at high mass loading.
- Ultrahigh specific capacitance with superior rate performance has been achieved.
- The asymmetric supercapacitor cell has been assembled.
- The cell delivers superior capacitive performance at high mass loading.

GRAPHICAL ABSTRACT

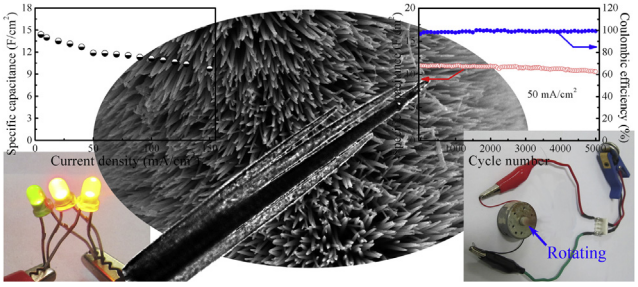

ARTICLE INFO

Article history:
Received 8 November 2013
Received in revised form
14 December 2013
Accepted 19 December 2013
Available online 31 December 2013

Keywords:
Nanotube arrays
Nickel cobalt sulfide
Supercapacitors
Asymmetric

ABSTRACT

Self-standing $NiCo_2S_4$ nanotube arrays have been *in situ* grown on Ni foam by the anion-exchange reaction and directly used as the electrode for supercapacitors. The $NiCo_2S_4$ nanotube in the arrays effectively reduces the inactive material and increases the electroactive surface area because of the ultrathin wall, which is quite competent to achieve high utilization efficiency at high electroactive materials mass loading. The $NiCo_2S_4$ nanotube arrays hybrid electrode exhibits an ultrahigh specific capacitance of 14.39 F cm^{-2} at 5 mA cm^{-2} with excellent rate performance (67.7% retention for current increases 30 times) and cycling stability (92% retention after 5000 cycles) at a high mass loading of 6 mg cm^{-2}. High areal capacitance (4.68 F cm^{-2} at 10 mA cm^{-2}), high energy density (31.5 Wh kg^{-1} at 156.6 W kg^{-1}) and high power density (2348.5 W kg^{-1} at 16.6 Wh kg^{-1}) can be achieved by assembling asymmetric supercapacitor with reduced graphene oxide at a total active material mass loading as high as 49.5 mg. This work demonstrates that $NiCo_2S_4$ nanotube arrays structure is a superior electroactive material for high-performance supercapacitors even at a mass loading of potential application-specific scale.

1. Introduction

Supercapacitors have drawn intensive research attention as ideal energy storage devices for applications such as electric vehicles and digital communications in view of their significant advantages of fast charging and discharging, long lifespan and high power density [1–3]. Generally, the performance of supercapacitors is mainly determined by properties of the electrode materials, so there is an extensive research on various electroactive materials so as to improve the performance of supercapacitors. Up to now, numerous electrode materials, including carbon-based materials [4,5],

* Corresponding author. Tel./fax: +86 27 87544472.
E-mail address: jiangjj@mail.hust.edu.cn (J. Jiang).

0378-7753/$ – see front matter © 2013 Elsevier B.V. All rights reserved.
http://dx.doi.org/10.1016/j.jpowsour.2013.12.092

transition metal compounds [6–9], and conducting polymers [10], have been well explored. Unfortunately, the poor performance of the electrode materials, such as the low specific capacitance in carbon based materials, the low conductivity in transition metal oxides, the high cost of RuO_2, and the poor cycling stability in conducting polymers, these respective fatal disadvantage impedes their practical applications. Therefore, it is desirable to seek other novel and efficient electrode materials so as to further improve the performance of supercapacitors.

Recently, ternary nickel cobalt sulphide, $NiCo_2S_4$, have been demonstrated to be a promising electrode material for supercapacitors. It is reported that $NiCo_2S_4$ possesses richer redox reactions than the corresponding binary nickel sulphide (NiS) and cobalt sulphide (Co_9S_8), and exhibits a major advantage over $NiCo_2O_4$ in terms of higher conductivity [11]. However, only $NiCo_2S_4$ powder has been synthesized by a hydrothermal method [11–13]. The traditional slurry-derived electrode used for electrochemical evaluation seriously limits the capacitive performance of the electroactive $NiCo_2S_4$ because of the increased "dead surface" [14]. Therefore, it is necessary to grow the $NiCo_2S_4$ directly on conductive substrate to facilitate the efficient utilization of $NiCo_2S_4$ for energy storage.

To increase the utilization efficiency of the electroactive, numerous nanostructures, such as various nanowire arrays [15–17] and nanosheets arrays [14,18,19], have been directly grown on conductive substrate to form an integrated electrode for electrochemical evaluation. In despite of the promising performance, the electroactive material in these arrays structures is too low (less than 2 mg cm^{-2}) to meet their practical applications. The utilization efficiency of the electroactive material usually decreases as the mass loading increasing. In the case of nanowire arrays, for example, there is an accompanied growth in the nanowire diameters and lengths when increase the electroactive materials to high mass loading per area [20,21]. Due to the limited diffusion distance of electrolyte ions, the electroactive materials in the inner nanowires will not be involved in the redox reaction and thus become "dead" or "inactive". So increasing the utilization efficiency of electroactive material at high mass loading is still a challenge. Nanotube structure can effectively reduce the inner inactive material and increase the electroactive surface area. Meanwhile, nanotube structure provides electrolyte ions penetrate into the electrode material from the inner nanotube surface, which will greatly increase the total diffusion distance. Therefore, by way of the nanotube arrays structure *in situ* grew on conductive Ni foam substrate to obtain a high mass loading may realize outstanding utilization efficiency.

Based on the above considerations, we develop a facile method using the anion-exchange reaction to grow $NiCo_2S_4$ nanotube arrays on Ni foam. This is the first trial to extend the anion-exchange reaction to grow nanotube arrays structure. After the electrochemical evaluation of the hybrid structure, the hybrid electrode can maintain ultrahigh specific capacitance even at a high mass loading of 6 mg cm^{-2} and achieve ultrahigh areal capacitance. Our work presents the first example of the increase of a single electroactive material to high mass loading while maintaining the superior specific capacitance, which is vital to achieve the potential practical applications of electroactive materials.

2. Experimental

2.1. Preparation of $NiCo_2(CO_3)_{1.5}(OH)_3$ nanowire arrays

All the reagents used in the experiment were of analytical grade and used without further purification. Prior to the synthesis, Ni foam (2 cm × 4 cm in rectangular shape) was first treated by acetone to clean the surface. Then, the Ni foam was immersed into a 3 M HCl solution for 15 min to remove the surface oxide layer. Finally, the Ni foam was washed thoroughly with deionized water and absolute ethanol. The $NiCo_2(CO_3)_{1.5}(OH)_3$ nanowire arrays supported on the Ni foam was prepared by a simple hydrothermal method. In a typical procedure, 8 mmol of $CoCl_2 \cdot 6H_2O$, 4 mmol of $NiCl_2 \cdot 6H_2O$ and 12 mmol of urea were dissolved in 60 ml deionized water to form a clear pink solution. The solution was transferred into an 80 ml Teflon-lined stainless steel autoclave. A piece of the pre-treated Ni foam was put into the autoclave. The autoclave was sealed and kept in an oven at 120 °C for 6 h. After cooling down to the room temperature, the $NiCo_2(CO_3)_{1.5}(OH)_3$ nanowire arrays supported on Ni foam was obtained and washed with deionized water and ethanol.

2.2. Preparation of $NiCo_2S_4$ nanotube arrays

The $NiCo_2S_4$ nanotube arrays were prepared by hydrothermal treating the as-obtained $NiCo_2(CO_3)_{1.5}(OH)_3$ nanowire arrays with sodium sulphide (Na_2S) under hydrothermal environment. Briefly, the $Na_2S \cdot 9H_2O$ was first dissolved in 60 ml deionized water in an 80 ml Teflon container, followed by addition of the $NiCo_2(CO_3)_{1.5}(OH)_3$ nanowire arrays supported on Ni foam. Then the autoclave was heated to 160 °C for 6 h. After cooling down to room temperature, the $NiCo_2S_4$ nanotube arrays on Ni foam was obtained and washed with deionized water and ethanol, then the sample was dried at 60 °C for 24 h.

2.3. Preparation of $NiCo_2O_4$ nanowire arrays

The $NiCo_2O_4$ nanowire arrays supported on Ni foam used in the comparative experiment were synthesized by annealing the as-obtained $NiCo_2(CO_3)_{1.5}(OH)_3$ nanowire arrays on Ni foam in air atmosphere at 400 °C for 3 h.

2.4. Preparation of RGO nanosheets

Briefly, graphene oxide (GO) nanosheets were firstly prepared by chemical exfoliation of natural graphite powders according to the well-established Hummers method, the detailed experiment process can be found elsewhere [22,23]. After repeated washing with water by centrifugation for several times, the GO was dispersed in water by ultrasonication. Then the suspension was diluted with a concentration of ~2 mg ml^{-1} for the following experiment. The reduced graphene oxide (RGO) nanosheets were prepared by hydrothermal reduction of the GO nanosheets. Typically, 60 ml of the GO aqueous dispersion containing about 120 mg of GO in an 80 ml Teflon-lined stainless steel autoclave was heated in an oven at 180 °C and kept at this temperature for 6 h. After cooling down to room temperature, the RGO sample was washed by vacuum filtration and collected by freeze-drying.

2.5. Materials characterization

The products were characterized by X-ray diffraction (XRD, Philips X'Pert Pro; Cu Kα, $\lambda = 0.1542$ nm), scanning electron microscopy (SEM, FEI Quanta 200 and Sirion 200), high-resolution transmission electron microscopy (HRTEM, JEOL JEM-2100F) and the X-ray fluorescence probe (XRF, EDAX Inc. Eagle III).

2.6. Electrochemical measurements

In half-cell tests, the electrochemical tests were conducted in a three-electrode glass cell with 6 M KOH as the aqueous electrolyte. Platinum foil and Hg/HgO electrodes were used as counter and reference electrodes, respectively. The Ni foam supported $NiCo_2S_4$

nanotube arrays or $NiCo_2O_4$ nanowire arrays is cut into 1 cm × 1 cm in quadrate shape and serves directly as the working electrode. To reduce the volume of the electrode, the $NiCo_2S_4$–Ni foam is sandwiched between two pieces of Ni foam and pressed at 3 MPa. The mass of $NiCo_2S_4$ active material in every electrode (~1 cm^2 in area) is ~6 mg. The electrodes were first activated by several CV cycles until the CV curves remained stable. In full cell tests, the asymmetric supercapacitor cell was assembled to measure the device performances. The electrochemical measurements were performed using a stainless steel two-electrode cell (Hefei Kejing Mater. Technol. CO., LTD). The Ni foam supported $NiCo_2S_4$ nanotube arrays is directly used as the positive electrode and the hydrothermal reductive RGO nanosheets serve as the negative electrode. The negative electrode was prepared by the traditional slurry coating method. Briefly, active material, acetylene black and poly(tetrafluoroethylene) were first mixed in a mass ratio of 80:10:10 to obtain a slurry. Due to the large amount of RGO in the negative electrode, the slurry was drop-dried into five pieces of Ni foam (1 cm × 1 cm) at 80 °C, then those five Ni foam were overlapped and pressed together at a pressure of about 10 MPa. The two asymmetric supercapacitor cells used to drive the LEDs and motor were assembled using CR 2025-type coin cells.

All of the electrochemical measurements were performed by a CHI 660D electrochemical workstation. The area specific capacitance of the hybrid electrode was calculated from the GCD curves by the equation: $C = I\Delta t/(S\Delta V)$, where C is the specific capacitance of the electrode (F cm^{-2}), I is the discharging current (A), Δt is the discharging time (s), S is the area of the electrode (cm^2) and ΔV is the discharging potential range (V).

The mass loading for the negative electrode was determined by balancing the charges stored in each electrode. Generally, the charges stored by positive and negative electrode can be determined by $q_+ = C_+ \times \Delta E \times S$ and $q_- = C_- \times \Delta E \times m$, where C_+, C_- represent the specific capacitance of positive electrode (F cm^{-2}) and negative electrode (F g^{-1}), respectively; ΔE is the potential range (V), S is the area of the positive electrode (cm^2); m is the weight of the active material in negative electrode (g). The charges are balanced by the equation of $q_+ = q_-$, where q_+ and q_- represent the charges stored in the positive and negative electrode, respectively.

3. Results and discussion

3.1. Synthesis and characterization of the $NiCo_2S_4$ nanotube arrays

The $NiCo_2S_4$ nanotube arrays on Ni foam were synthesized via a two-step process, as illustrated in Scheme 1 in Fig. 1. Typically, the $NiCo_2(CO_3)_{1.5}(OH)_3$ nanowire arrays supported on Ni foam were firstly *in situ* grew on Ni foam by hydrothermal treating Ni^{2+} and Co^{2+} in the presence of urea (step I in Scheme 1, Fig. 1). For the next step, the as-fabricated $NiCo_2(CO_3)_{1.5}(OH)_3$ nanowire arrays on Ni foam are hydrothermally converted to the $NiCo_2S_4$ nanotube arrays counterpart by reacting with sodium sulphide (Na_2S) (step II in Scheme 1, Fig. 1). In this process, the well-known anion-exchange reaction mechanism, which has been used to grow various hollow nanoparticles and nanotubes [24,25], can best explain the conversion of the $NiCo_2(CO_3)_{1.5}(OH)_3$ nanowires into $NiCo_2S_4$ nanotubes while completely maintaining the array structure on Ni foam (Scheme 2, Fig. 1). First, S^{2-} anions in the solution exchange with CO_3^{2-} and OH^- anions of $NiCo_2(CO_3)_{1.5}(OH)_3$ to form $NiCo_2S_4$ at the surface of the nanowires. The CO_3^{2-} and OH^- anions can react with hydrogen cations in the solution to produce CO_2 and H_2O. In the next step, the spontaneously outward diffusion of the inner $NiCo_2(CO_3)_{1.5}(OH)_3$ to the external surface of the nanowires provides a source of $NiCo_2(CO_3)_{1.5}(OH)_3$ for further anion exchange and the growth of the $NiCo_2S_4$. Meanwhile, inward ion diffusion is limited for the anion exchange reaction, which has been proved by the Alivisatos research group [25]. The continuous outward diffusion of internal $NiCo_2(CO_3)_{1.5}(OH)_3$ results in the generation of void space inside the starting 1D nanowires. When the $NiCo_2(CO_3)_{1.5}(OH)_3$ component has been completely converted into $NiCo_2S_4$, the starting 1D nanowires become hollow nanotubes. Strikingly, due to the utilization of nanowire arrays as the precursor, this is the first attempt to extend the anion-exchange reaction to grow nanotube arrays structure.

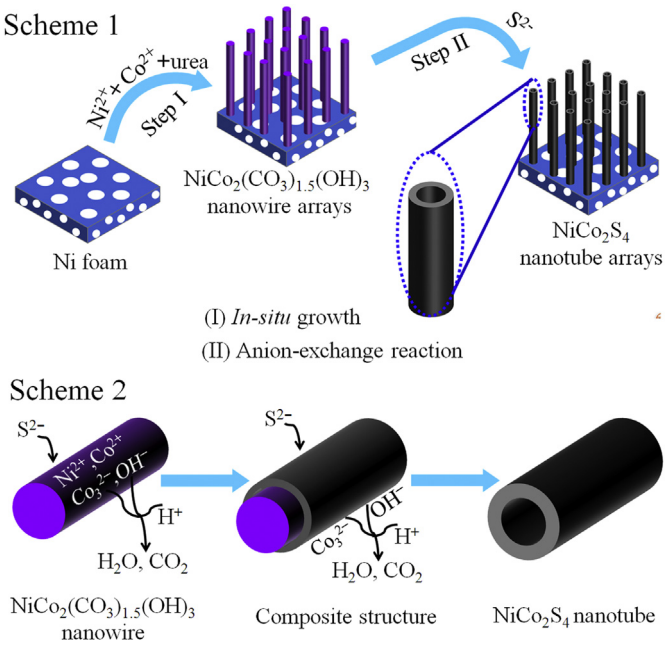

Fig. 1. Scheme 1. Schematic illustrating the formation process of the $NiCo_2S_4$ nanotube arrays on Ni foam. **Scheme 2**. Schematic illustration of the formation of $NiCo_2S_4$ nanotube through the anion-exchange reaction of the $NiCo_2(CO_3)_{1.5}(OH)_3$ nanowires with S^{2-}.

Fig. 2a shows the representative low-magnification SEM image of the $NiCo_2S_4$ on Ni foam. Obviously, the $NiCo_2S_4$ is uniform covered on the Ni foam while completely maintaining the 3D grid structure of the pristine Ni foam. By a closer examination of the sample in Fig. 2b–d, it is found that numerous slim nanowires vertically aligned on the Ni foam to form a homogeneously nanowire arrays. Obviously, the $NiCo_2S_4$ nanowire arrays completely maintain the arrays structure of $NiCo_2(CO_3)_{1.5}(OH)_3$ precursor (Fig. S1). The detailed morphology and hollow structure can be confirmed by HRTEM, as shown in Fig. 3. Apparently, the $NiCo_2S_4$ nanowires are hollow internally (Fig. 3a and b), indicating the successful preparation of $NiCo_2S_4$ nanotube arrays on Ni foam. By a closer examination of the nanotube wall in Fig. 3c and d, it is found that the $NiCo_2S_4$ is porous with numerous pores located at the nanotube. These pores serve as the outward diffusion pathway for the $NiCo_2(CO_3)_{1.5}(OH)_3$ in the anion-exchange reaction. The $NiCo_2S_4$ nanotube shows a very rough surface (Fig. 3e and f) and a very thin wall (Fig. 3g), which is very effective to increase the electroactive sites. The thickness of the nanotube wall is about 15 nm, as shown in Fig. 3g. The selected-area electron diffraction (SAED) pattern in the inset of Fig. 3f demonstrates polycrystalline nature of the $NiCo_2S_4$ nanotube, which is composed by domains of nanocrystallites (Fig. 3h). The lattice fringes in Fig. 3i can be assigned to the (311) crystal plane, indicating the successful formation of crystalline $NiCo_2S_4$.

The as-synthesized sample was further confirmed by the XRD and XRF measurements. Fig. 4a shows the XRD pattern of the as-

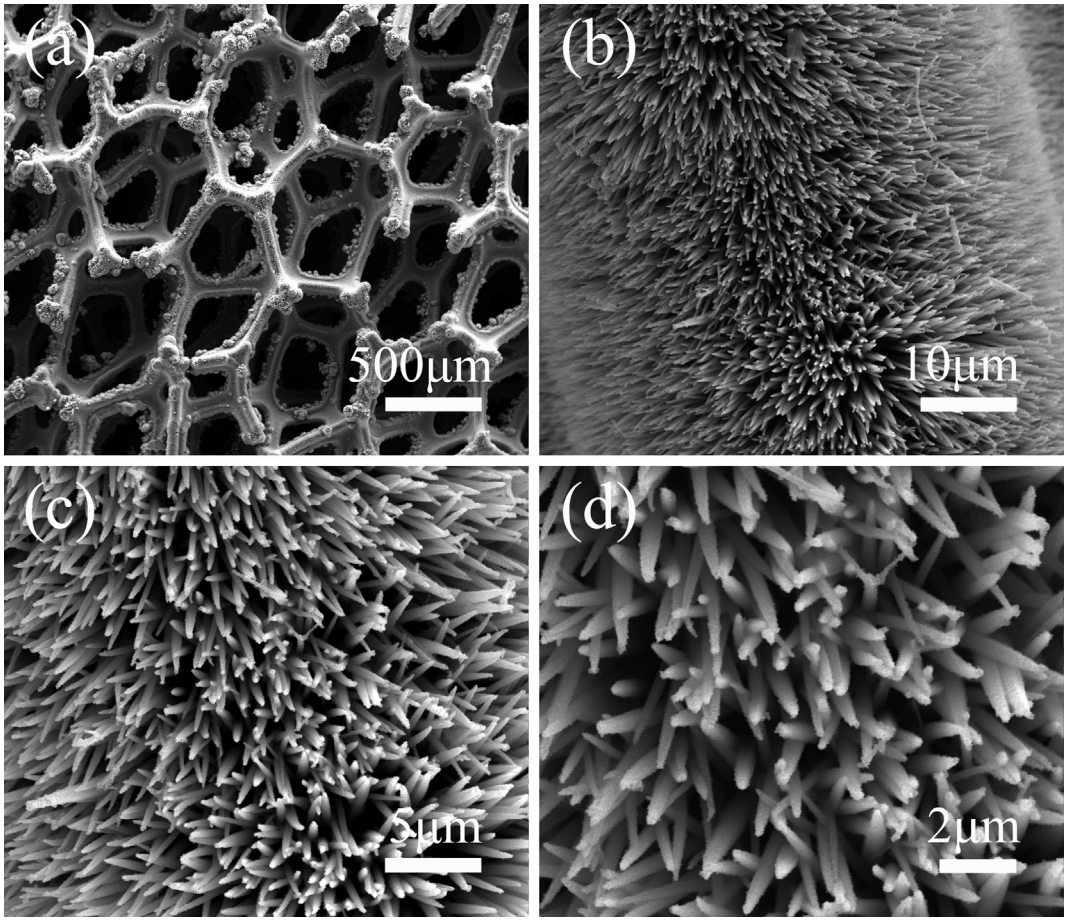

Fig. 2. (a–d) SEM images of the $NiCo_2S_4$ nanotube arrays on Ni foam.

synthesized sample. Except for the diffraction peaks from Ni foam, all the other diffraction peaks can be assigned to the cubic type $NiCo_2S_4$ (JCPDS Card no. 43-1477), indicating successful formation of the $NiCo_2S_4$ phase. The existence of S element in the sample can be further verified by XRF measurement (Fig. 4b), which signifies the successful conversion of the precursor into the sulphide counterpart. To avoid the XRF signal from the Ni foam substrate, the $NiCo_2S_4$ nanotubes were scraped from Ni foam for XRF test. The element ratio of Ni, Co and S is 1:1.997:3.657, matching well with the formula of $NiCo_2S_4$.

3.2. Electrochemical performances of the $NiCo_2S_4$ nanotube arrays hybrid electrode

The as-synthesized $NiCo_2S_4$ nanotube arrays supported on Ni foam were directly applied as the binder-free and conductive-agent-free electrodes in a three-electrode configuration with 6 M KOH as the electrolyte. The mass of $NiCo_2S_4$ nanotubes used in every working electrode is 6 mg and the geometric area of each electrode is 1 cm^2. Obviously, the mass loading of the $NiCo_2S_4$ nanotubes in the working electrode is several times higher than various electroactive arrays structure reported previously [14,15,17–19]. In comparative experiment, the $NiCo_2O_4$ nanowire arrays on Ni foam with comparable mass loading have also been prepared by annealing the same $NiCo_2(CO_3)_{1.5}(OH)_3$ nanowire arrays in air atmosphere following previous reported method [15–17]. Meanwhile, the electrochemical properties of Ni foam without any electroactive material was also measured. Fig. 5a and b shows the cyclic voltammetry (CV) and galvanostatic charge-discharge (GCD) cures at 5 mV s^{-1} and 10 mA cm^{-2}, respectively. Obviously, the CV integrated area and the discharge time of the $NiCo_2S_4$ electrode are significantly higher than those of $NiCo_2O_4$ and Ni foam, signifying the outstanding performance of the as-synthesized $NiCo_2S_4$ nanotube arrays.

The electrochemical properties of the $NiCo_2S_4$ nanotube arrays were evaluated by CV and GCD measurements. Fig. 5c is the representative CV curves at various sweep rates ranging from 1 to 10 mV s^{-1}. Obviously, the redox peaks in each CV curve demonstrate the pseudocapacitive properties of the $NiCo_2S_4$ nanotube arrays-Ni foam electrode. The distinct redox peaks in all CV curves can be attributed to the reversible redox reactions of Ni^{2+}/Ni^{3+}, Co^{2+}/Co^{3+} and Co^{3+}/Co^{4+} transitions based on the following equations [26]:

$$NiCo_2S_4 + 2OH^- = NiS_{4-2x}OH + 2CoS_xOH + 2e^-$$

$$CoS_xOH + OH^- = CoS_xO + H_2O + e^-$$

GCD test is also conducted to evaluate the potential window and the capacitive performance of the hybrid electrode. Fig. 5d and e presents the GCD curves of $NiCo_2S_4$ electrode at various current densities varying from 5 to 150 mA cm^{-2} with a potential window ranging from 0 to 0.55 V (vs. Hg/HgO reference electrode). The distinct plateau regions in the GCD curves can further demonstrate the pseudocapacitive characteristics of the $NiCo_2S_4$, which match very well with the redox peaks in the CV curves. The multiple plateaus in every charge or discharge process indicate the multistep

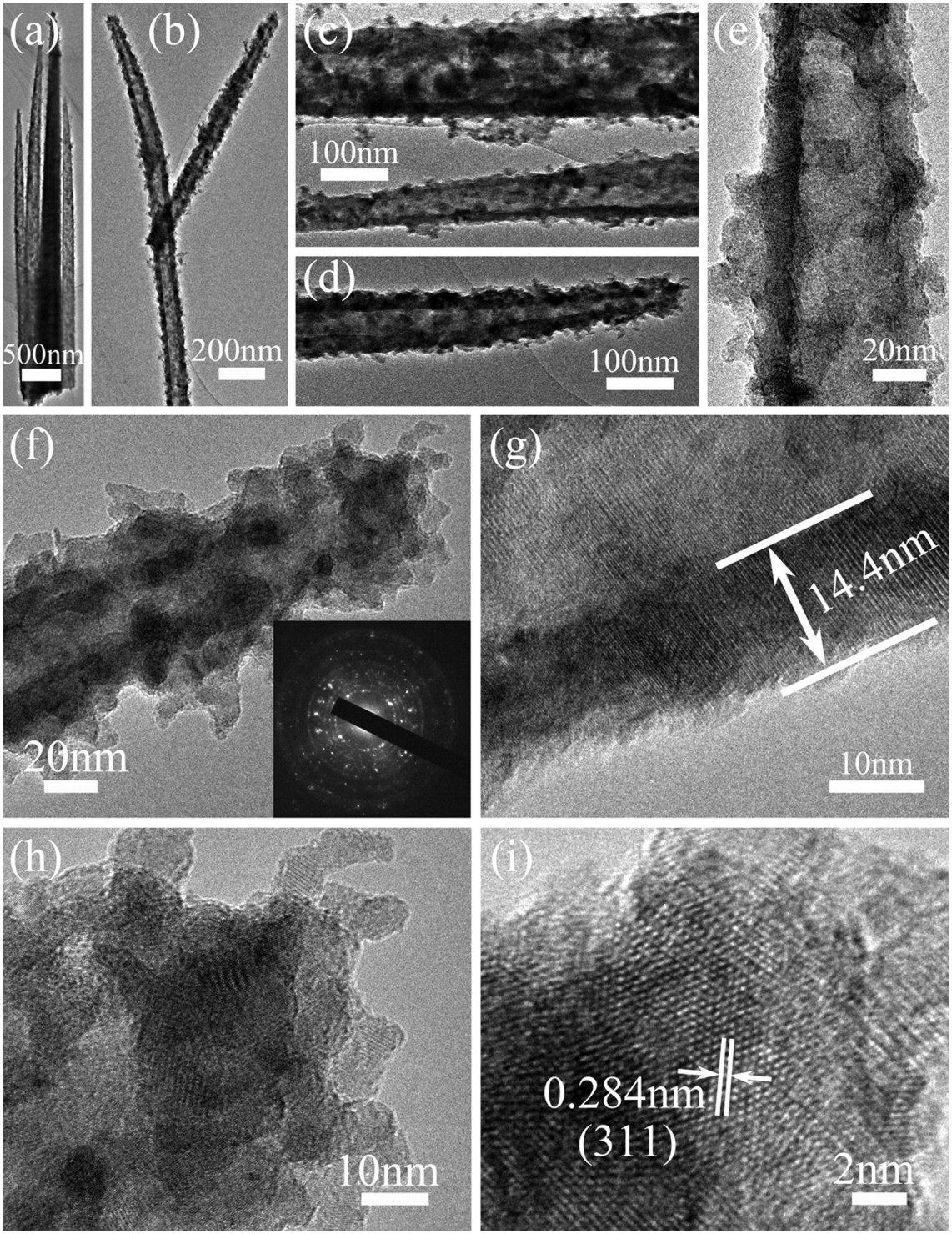

Fig. 3. (a–g) TEM images, (h, i) HRTEM images of the $NiCo_2S_4$ nanotubes scraped from Ni foam. The inset of (f) is an SAED pattern of the $NiCo_2S_4$ nanotube.

redox reactions of the active materials because of the coexistence of the Ni ions and Co ions. The specific capacitance can be directly calculated from the GCD curves and the corresponding results are plotted in Fig. 5f. Apparently, at a comparable mass loading, $NiCo_2S_4$ nanotube arrays deliver a much higher capacitive performance than the $NiCo_2O_4$ nanowire arrays at the whole measured current density range. Remarkably, the specific capacitance of the $NiCo_2S_4$ nanotube arrays as high as 14.39 F cm^{-2} at a current density of 5 mA cm^{-2}, corresponding to a specific capacitance of about 2398 F g^{-1}, such high a pseudocapacitance is not observed for electroactive $NiCo_2S_2$ till now [11–13]. Obviously, the $NiCo_2S_4$ nanotube arrays on Ni foam exhibit much higher specific capacitance than various previous reported electroactive materials on Ni foam, such as $NiCo_2O_4$ [27,28], $Ni(OH)_2$ [29], Co_3O_4 [30]. The ultrahigh specific capacitance of the hybrid electrode can be ascribed to the specific nanotube arrays structure. Such high a specific capacitance at high mass loading can push the areal capacitance to a high level. The $NiCo_2S_4$ nanotube arrays deliver a much higher

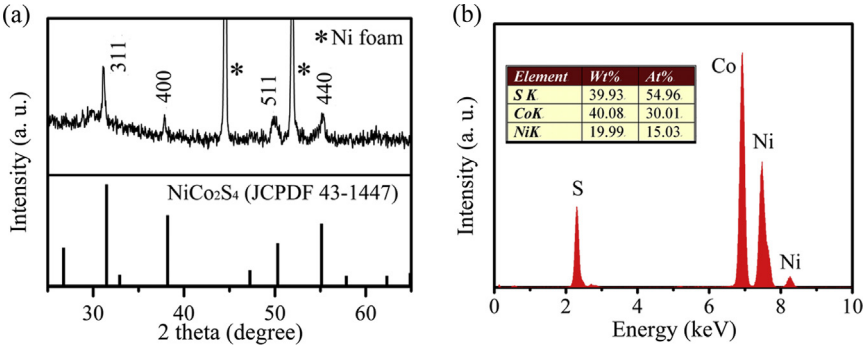

Fig. 4. (a) XRD and (b) XRF patterns of the $NiCo_2S_4$ nanotube arrays.

areal capacitance than, to the best of our knowledge, all the reported single electroactive materials at low or comparable mass loading [14–19], and show even a higher areal capacitance than various electroactive materials with about three times mass loadings, such as Co_3O_4 nanowire arrays on Ni foam (11.9 F cm^{-2} at 16 mg cm^{-2}) [20], and Ni–Al layered double hydroxide on Ni foam (14.0 F cm^{-2} at 20 mg cm^{-2}) [31]. The specific capacitance of the hybrid electrode can still remain 9.74 F cm^{-2} at a current density as high as 150 mA cm^{-2}, corresponding to 67.7% of the capacitance retention for current density increase 30 times, which is much higher than the $NiCo_2O_4$ nanowire array (29.7% of the capacitance retention for current density increase 30 times), as shown in Fig. 5f. The high capacitance retention demonstrates the fast kinetics of ion and electron transport, which can be attributed to the high conductivity of $NiCo_2S_4$ and the ion diffusion-favoured nanotube arrays structure. The cycling stability of the $NiCo_2S_4$ electrode is quite

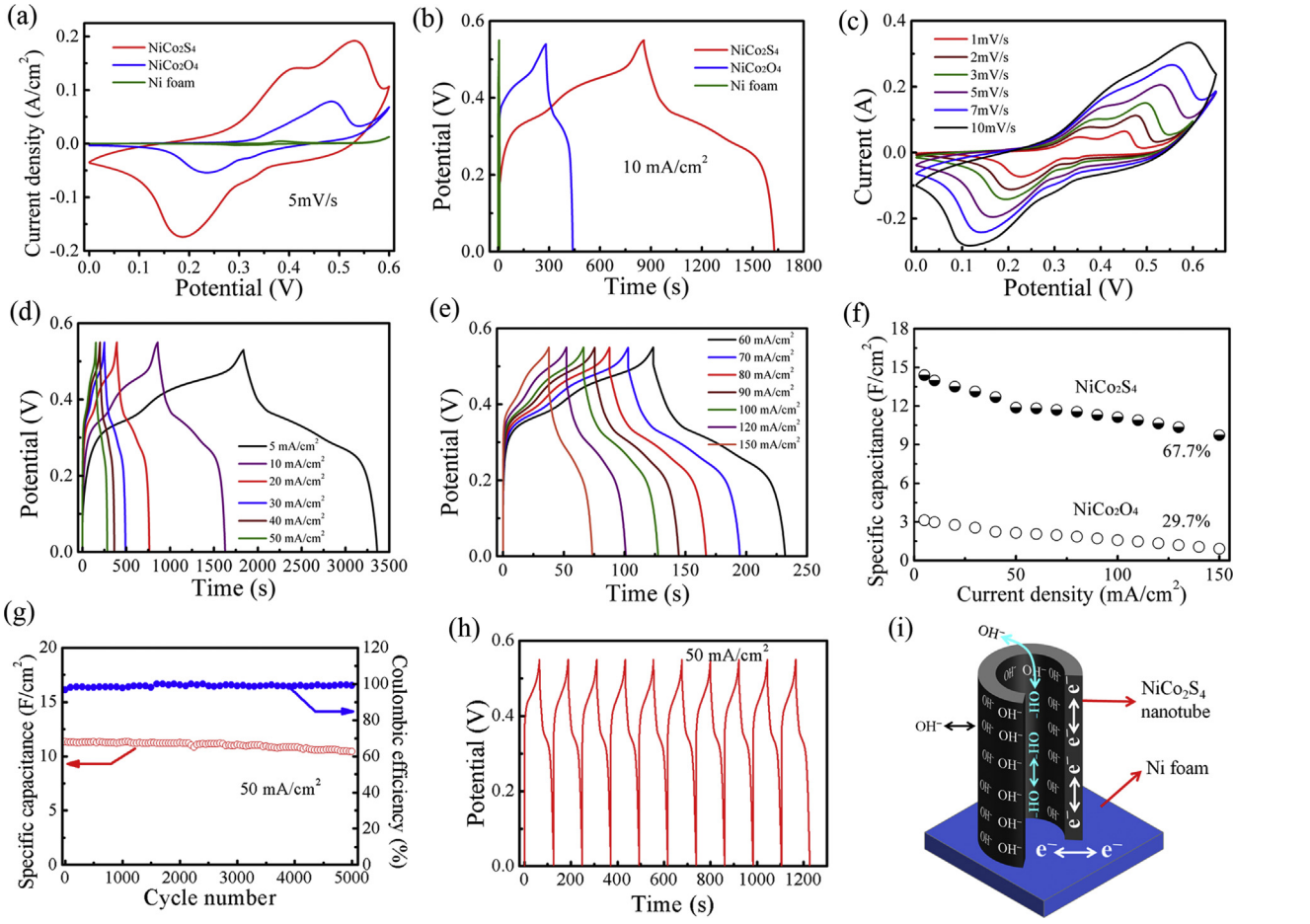

Fig. 5. (a) CV curves and (b) GCD curves of the $NiCo_2O_4$ nanowire arrays, $NiCo_2S_4$ nanotube arrays and Ni foam measured at a scan rate of 5 mV s^{-1} and at a current density of 10 mA cm^{-2}. (c) CV curves and (d, e) GCD curves of the $NiCo_2S_4$ nanotube arrays on Ni foam with different rates. (f) Specific capacitance as a function of the current density of the $NiCo_2S_4$ and $NiCo_2O_4$ arrays on Ni foam. (g) Cycle performance and Coulombic efficiency for the $NiCo_2S_4$ nanotube arrays on Ni foam at a current of 50 mA cm^{-2}. (h) Ten GCD curves measured after the 5000 cycles. (i) Illustration of the electrons and ions transport pathways of the $NiCo_2S_4$ nanotube arrays-Ni foam hybrid electrode: the electrolyte ions can diffuse into/out the inner side of the nanotube, penetrate into/out of the $NiCo_2S_4$ tube wall from the inner and out sides of the nanotube; the electrons can fast transfer between Ni foam and the $NiCo_2S_4$, and transport along the nanotube wall to the electroactive sites.

stable and 92% of the specific capacitance can still be retained after 5000 cycles (Fig. 5g). The capacitance retention is apparently much higher than those of various binary sulphides, such as NiS and CoS_2 [32–34]. The hybrid electrode shows a high electrochemical reversibility with nearly 100% Coulombic efficiency can be maintained (Fig. 5g). Fig. 5h is the last 10 cycles of charging and discharging at a current density of 50 mA cm^{-2}, and the Coulombic efficiency is about 99% for each cycle even after 5000 cycles cycling test.

The superior supercapacitive performance of the $NiCo_2S_4$ arrays on Ni foam compared to the $NiCo_2O_4$ arrays can be attributed to the outstanding capability of $NiCo_2S_4$ electroactive material and the unique nanotube morphology. The merits of as-prepared $NiCo_2S_4$ electroactive material are as follows: (1) based on the work by our group previously [11], the $NiCo_2S_4$ possess even a higher conductivity compared to the $NiCo_2O_4$, so the $NiCo_2S_4$ nanotube provide facilitate pathway for the electron transport along the nanotube wall, as illustrated in Fig. 5i. As a result, superior high-rate performance can be achieved; (2) the $NiCo_2S_4$ electroactive material is prepared using a two-step solution method, avoiding the use of calcination process at elevated temperature. Consequently, some chemical functional groups or dangling bonds, such as −OH and −SH, are retained, which can improve the wettability of active material surfaces. Therefore, the electrolyte ions can well accessible and contact to the $NiCo_2S_4$ surface during the electrochemical process, which is beneficial for the full utilization of the electroactive sites on the $NiCo_2S_4$ nanotubes; (3) The $NiCo_2S_4$ can effective maintain low-crystalline due to the annealing-free preparation method, resulting in a high specific surface area and structural disorder [35,36], which is indispensable for good supercapacitive performance. Based on the analysis above, the as-obtained $NiCo_2S_4$ shows even much more merits than the extensively studied $NiCo_2O_4$. Different from the $NiCo_2O_4$ nanowire arrays, the as-prepared $NiCo_2S_4$ in the arrays structure shows nanotube morphology. Electroactive material with nanotube morphology is better than nanowires because (1) nanotube can effectively alleviate the volume change during the ion insertion/desertion process, resulting in an improved cycling stability; (2) nanotube has much high specific surface, which can provide more electroactive sites for electrochemical storage. In our work, the as-prepared $NiCo_2S_4$ nanotube is reproduced from the $NiCo_2(CO_3)_{1.5}(OH)_3$ nanowire precursor base on the anion-exchange reaction, about twice the surface area of the nanowire can be achieved. Meanwhile, numerous hole on the nanotube walls (Fig. 3c and d) can facilitate the electrolyte ions penetrate into the inside range of nanotube. In this way, the inner surface of the $NiCo_2S_4$ can be utilized for energy storage. So compared to nanowire morphology, the as-synthesized $NiCo_2S_4$ nanotubes can achieve better capability. Besides, even at a high mass loading, the $NiCo_2S_4$ nanotube retains a thin wall thickness (Fig. 3g). Based on a previous study, the maximal electrolyte ions diffusion length is about 20 nm [37], greater than the thickness of nanotube wall (~15 nm). The nanotube morphology provides two directions for the electrolyte ions penetrate into the electroactive material, as shown schematically in Fig. 5i, and thus reduces the diffusion distance, which contributes to the full utilization of the $NiCo_2S_4$. Based on these reasons, the as-synthesized $NiCo_2S_4$ nanotube arrays on Ni foam exhibit much higher capacitive performance than $NiCo_2O_4$.

3.3. Electrochemical performances of the RGO//$NiCo_2S_4$ asymmetric supercapacitor devices

To further demonstrate the superior capacitive performance of the high mass-loaded $NiCo_2S_4$ nanotube arrays on Ni foam, an asymmetric supercapacitor cell was assembled using the $NiCo_2S_4$ nanotube arrays and the reduced graphene oxide (RGO) as positive and negative electrodes (Fig. 6a). Fig. 6b shows the CV curves of $NiCo_2S_4$ nanotube arrays and the RGO with a scan rate of 5 mV s^{-1} in 6 M KOH. The specific capacitance of $NiCo_2S_4$ and RGO calculated from the CV curves in Fig. 6b are 14.27 F cm^{-2} and 197 F g^{-1}, respectively. Based on the specific capacitance values and potential windows, the mass of RGO is determined to be 43.5 mg to balance the charges stored in the $NiCo_2S_4$ electrode (~1 cm^2), corresponding to a mass ratio of about 7.2:1 between RGO and $NiCo_2S_4$. Such a high mass ratio in turn demonstrates the ultrahigh capability of the $NiCo_2S_4$ nanotube arrays on Ni foam. Fig. 6c shows the representative GCD curves of the asymmetric supercapacitor at various current densities. The specific capacitance was calculated from the as-measured GCD curves and the results are plotted in Fig. 6d. Remarkably, the asymmetric supercapacitor device achieves a capability of 4.68 F cm^{-2} at a current density of 10 mA cm^{-2}. After 15-time increase in the current density, 2.46 F cm^{-2} of the specific capacitance can be still remained, corresponding to 52.6% of the specific capacitance retention. The Ragone plot derived from the GCD curves is presented in Fig. 6e. The asymmetric supercapacitor exhibits a high areal energy density of 15.6 Wh m^{-2} at an areal power density of 77.5 W m^{-2}, to the best of our knowledge, this is the highest areal energy density reported for various asymmetric supercapacitors. The gravimetric energy density and power density of our supercapacitor device are further provided in Fig. 6f for ease of comparison with various reported supercapacitors with low mass loading. The energy of the asymmetric supercapacitor reaches 31.5 Wh kg^{-1} at a power density of 156.6 W kg^{-1}, and still remains 16.6 Wh kg^{-1} at a power density of 2348.5 W kg^{-1}. The energy density of our supercapacitor is much higher than the nickel cobaltite-graphene//AC asymmetrical supercapacitor (19.5 Wh kg^{-1} at about 100 W kg^{-1}) [38] at a comparable mass loading and much higher than various carbon based symmetric supercapacitors in aqueous electrolyte [39–41]. The high energy density can be attributed to the high specific capacitance or the large cell voltage. Meanwhile, our supercapacitor delivers a higher energy density than various Ni–Co compounds based asymmetric supercapacitors, including mesoporous $NiCo_2O_4$//AC (17.72 Wh kg^{-1}) [42], submicron/micron-sized $NiCo_2O_4$//AC (14.7 Wh kg^{-1} at 175 W kg^{-1}) [43], porous Ni–Co oxide//AC (12 Wh kg^{-1} at 95.2 W kg^{-1}) [44], Ni_xCo_{1-x} LDH–ZTO heterostructure//AC (23.7 Wh kg^{-1} at 284.2 W kg^{-1}) [45] and $NiCo_2O_4$–RGO composite//AC (23.3 Wh kg^{-1} at 324.9 W kg^{-1}) [46] asymmetric supercapacitors, and various other ternary compound based asymmetric supercapacitors, such as amorphous $NiWO_4$//AC (25.3 Wh kg^{-1} at 200 W kg^{-1}) [47], nano β-$NiMoO_4$–$CoMoO_4 \cdot xH_2O$ composites//AC (28 Wh kg^{-1} at 100 W kg^{-1} and 18 Wh kg^{-1} at 1000 W kg^{-1}) [48], and $CoMoO_4$–$NiMoO_4 \cdot xH_2O$ bundles//AC (24.95 Wh kg^{-1} at 164.5 W kg^{-1} and 15.54 Wh kg^{-1} at 1645.4 W kg^{-1}) [49] supercapacitors. All these attractive results demonstrate the outstanding supercapacitive performance of the $NiCo_2S_4$ nanotube arrays-Ni foam//RGO asymmetric supercapacitor even at an ultrahigh total mass loading of active materials as high as 49.5 mg. Such a high energy density is quite competent to drive the realistic low voltage devices. The two series connected asymmetric supercapacitor can simultaneously light 3 mm diameter yellow (1.97 V, 20 mA), red (2.03 V, 20 mA), and green (2.20 V, 20 mA) round light-emitting diodes (LEDs) (Fig. 6g). In the long-term lighting test, the device is able to power a red LED efficiently for 2 h (Fig. 6h). More attractively, the device can drive a motor (3 V, 80 mA) rapid rotation for about 1 min (Fig. 6i and Movie in Supporting information). These results are robust enough to demonstrate the outstanding performance of asymmetric supercapacitors and the electroactive material in practical applications.

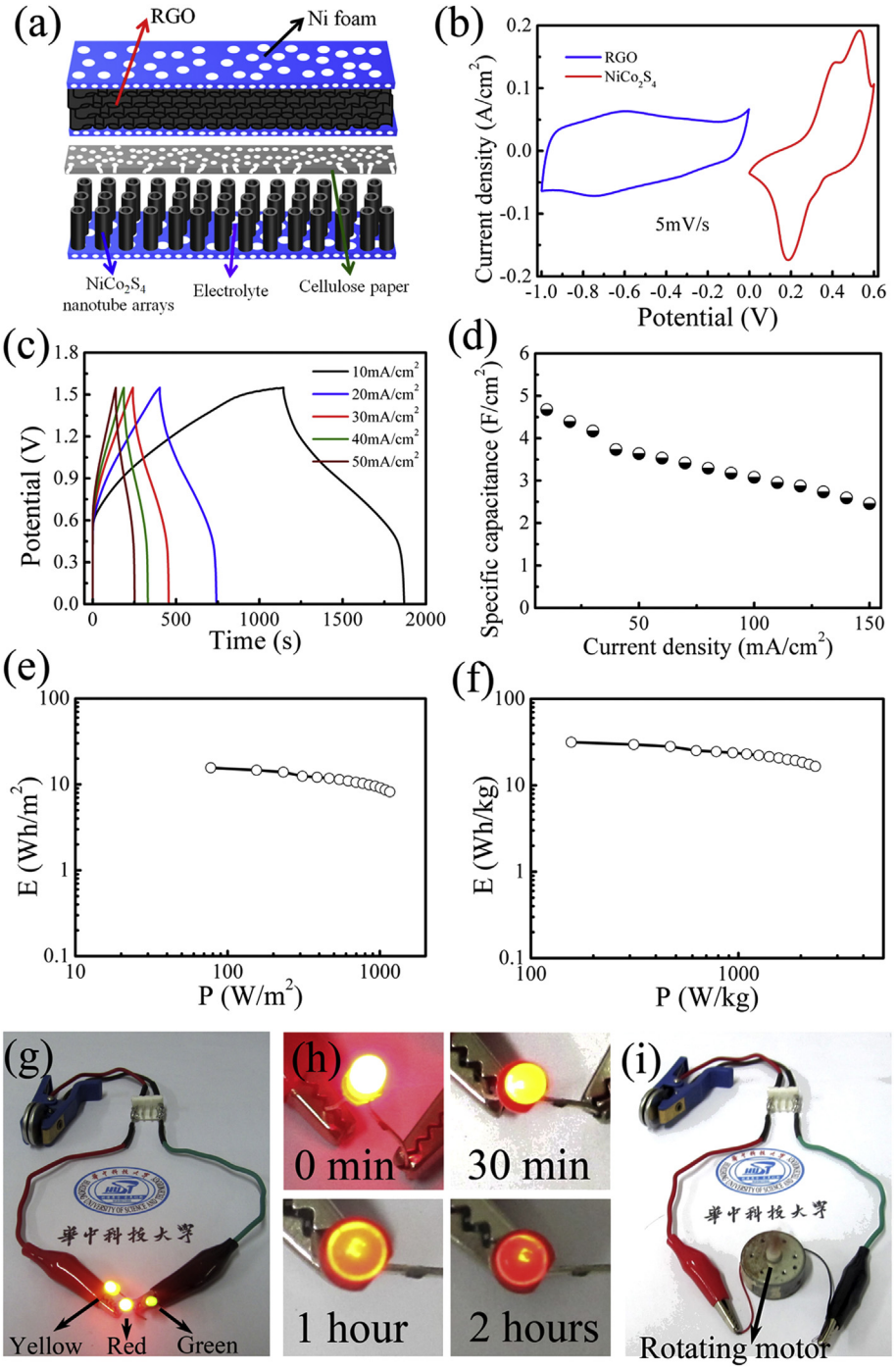

Fig. 6. (a) Schematic illustration of the asymmetric supercapacitor configuration. (b) CV curves of the RGO and $NiCo_2S_4$ nanotube arrays with a scan rate of 5 mV s^{-1} measured by a three-electrode configuration. (c) GCD curves of the asymmetric supercapacitor measure at different current densities from 10 to 150 mA cm^{-2}. (d) Specific capacitance as a function of the current density of the asymmetric supercapacitor. (e) Areal energy and power density and (f) Ragone plot of our device. Two assembled asymmetric supercapacitor is connected in series and used to drive the realistic low voltage devices: (g) parallel LEDs with different colours; (h) red LED at different lighting times; (i) a motor. (For interpretation of the references to colour in this figure legend, the reader is referred to the web version of this article.)

Supplementary video related to this article can be found online at http://dx.doi.org/10.1016/j.jpowsour.2013.12.092.

4. Conclusions

In summary, self-standing $NiCo_2S_4$ nanotube arrays on Ni foam have been synthesized based on the anion-exchange reaction. The hybrid electrode demonstrates an ultrahigh specific capacitance of 2398 F g^{-1} at a high $NiCo_2S_4$ mass loading of about 6 mg cm^{-2}, which is quite competent to push the areal capacitance of the electrode to a high level. The outstanding supercapacitive performance can be attributed to the superior capability of $NiCo_2S_4$ electroactive material and the specific nanotube array structure. An asymmetric supercapacitor based on the $NiCo_2S_4$ nanotube arrays-Ni foam hybrid electrode in aqueous electrolyte delivers high specific energy and power densities even at the total mass of the

electroactive materials as high as 49.5 mg, which is very capable of driving various realistic low voltage device including LED and motor. Our work demonstration of the $NiCo_2S_4$ nanotube arrays structure a promising electroactive material for high-performance supercapacitors even at high mass loading for the first time and provides a new and facile strategy to engineer advanced electroactive material with nanotube array structure.

Acknowledgements

This work is supported by the National Natural Science Foundation of China (nos. 61172003, 51102104 and 51302097) and Wuhan Planning Project of Science and Technology (no. 2013011801010594). The authors also thank the Analysis and Testing Center of HUST for samples testing support.

Appendix A. Supporting information

Supporting information related to this article can be found online at http://dx.doi.org/10.1016/j.jpowsour.2013.12.092.

References

[1] B.E. Conway, Electrochemical Supercapacitors: Scientific Fundamentals and Technological Applications, Kluwer Academic/Plenum Publishers, New York, 1999.
[2] M. Zhi, C. Xiang, J. Li, M. Li, N. Wu, Nanoscale 5 (2013) 72.
[3] P. Simon, Y. Gogotsi, Nat. Mater. 7 (2008) 845.
[4] A. Izadi-Najafabadi, T. Yamada, D.N. Futaba, M. Yudasaka, H. Takagi, H. Hatori, S. Iijima, K. Hata, ACS Nano 5 (2011) 811.
[5] J. Han, L.L. Zhang, S. Lee, J. Oh, K.S. Lee, J.R. Potts, J. Ji, X. Zhao, R.S. Ruoff, S. Park, ACS Nano 7 (2012) 19.
[6] G. Zhang, X.W. Lou, Sci. Rep. 3 (2013) 1470.
[7] H.C. Chen, J.J. Jiang, L. Zhang, T. Qi, D.D. Xia, H.Z. Wan, J. Power Sources 248 (2014) 28.
[8] B.P. Bastakoti, H.S. Huang, L.C. Chen, K.C.W. Wu, Y. Yamauchi, Chem. Commun. 48 (2012) 9150.
[9] S.K. Meher, G.R. Rao, J. Phys. Chem. C 115 (2011) 15646.
[10] K. Wang, J. Huang, Z. Wei, J. Phys. Chem. C 114 (2010) 8062.
[11] H.C. Chen, J.J. Jiang, L. Zhang, H.Z. Wan, T. Qi, D.D. Xia, Nanoscale 5 (2013) 8879.
[12] H.Z. Wan, J.J. Jiang, J.W. Yu, K. Xu, L. Miao, L. Zhang, H.C. Chen, Y.J. Ruan, CrystEngCommun 15 (2013) 7649.
[13] S. Peng, L. Li, C. Li, H. Tan, R. Cai, H. Yu, S. Mhaisalkar, M. Srinivasan, S. Ramakrishna, Q. Yan, Chem. Commun. (2013), http://dx.doi.org/10.1039/C3CC46034G.
[14] C. Yuan, J. Li, L. Hou, X. Zhang, L. Shen, X.W. Lou, Adv. Funct. Mater 22 (2012) 4592.
[15] Z. Lu, Z. Chang, J. Liu, X. Sun, Nano Res. 4 (2011) 658.
[16] Q. Wang, X. Wang, B. Liu, G. Yu, X. Hou, D. Chen, G. Shen, J. Mater. Chem. A 1 (2013) 2468.
[17] G.Q. Zhang, H.B. Wu, H.E. Hoster, M.B. Chan-Park, X.W. Lou, Energy Environ. Sci. 5 (2012) 9453.
[18] G. Zhang, X.W. Lou, Adv. Mater. 25 (2013) 976.
[19] C. Yuan, L. Yang, L. Hou, L. Shen, X. Zhang, X.W. Lou, Energy Environ. Sci. 5 (2012) 7883.
[20] Y. Gao, S. Chen, D. Cao, G. Wang, J. Yin, J. Power Sources 195 (2010) 1757.
[21] G. Wang, D. Cao, C. Yin, Y. Gao, J. Yin, L. Cheng, Chem. Mater. 21 (2009) 5112.
[22] N.I. Kovtyukhova, P.J. Ollivier, B.R. Martin, T.E. Mallouk, S.A. Chizhik, E.V. Buzaneva, A.D. Gorchinskiy, Chem. Mater. 11 (1999) 771.
[23] W.S. Hummers, R.E. Offeman, J. Am. Chem. Soc. 80 (1958) 1339.
[24] S. Zhuo, Y. Xu, W. Zhao, J. Zhang, B. Zhang, Angew. Chem. Int. Ed. 52 (2013) 8602.
[25] J. Park, H. Zheng, Y. Jun, A.P. Alivisatos, J. Am. Chem. Soc. 131 (2009) 13943.
[26] L. Mei, T. Yang, C. Xu, M. Zhang, L. Chen, Q. Li, T. Wang, Nano Energy 3 (2014) 36.
[27] X.Y. Liu, Y.Q. Zhang, X.H. Xia, S.J. Shi, Y. Lu, X.L. Wang, C.D. Gu, J.P. Tu, J. Power Sources 239 (2013) 157.
[28] X. Liu, S. Shi, Q. Xiong, L. Li, Y. Zhang, H. Tang, C. Gu, X. Wang, J. Tu, ACS Appl. Mater. Interfaces 5 (2013) 8790.
[29] M.S. Wu, K.C. Huang, Chem. Commun. 47 (2011) 12122.
[30] X. Xia, J. Tu, Y. Zhang, Y. Mai, X. Wang, C. Gu, Xi Zhao, RSC Adv. 2 (2012) 1835.
[31] J. Wang, Y. Song, Z. Li, Q. Liu, J. Zhou, X. Jing, M. Zhang, Z. Jiang, Energy Fuels 24 (2010) 6463.
[32] T. Zhu, Z.Y. Wang, S.J. Ding, J.S. Chen, X.W. Lou, RSC Adv. 1 (2011) 397.
[33] L. Zhang, H.B. Wu, X.W. Lou, Chem. Commun. 48 (2012) 6912.
[34] H.Z. Wan, X. Ji, J.J. Jiang, J.W. Yu, L. Miao, L. Zhang, S.W. Bie, H.C. Chen, Y.J. Ruan, J. Power Sources 243 (2013) 396.
[35] H.B. Li, M.H. Yu, F.X. Wang, P. Liu, Y. Liang, J. Xiao, C.X. Wang, Y.X. Tong, G.W. Yang, Nat. Commun. 4 (2013) 1894.
[36] T.Y. Wei, C.H. Chen, H.C. Chien, S.Y. Lu, C.C. Hu, Adv. Mater. 22 (2010) 347.
[37] C.C. Hu, K.H. Chang, M.C. Lin, Y.T. Wu, Nano Lett. 6 (2006) 2690.
[38] H. Wang, C.M.B. Holt, Z. Li, X. Tan, B.S. Amirkhiz, Z. Xu, B.C. Olsen, T. Stephenson, D. Mitlin, Nano Res. 5 (2012) 605.
[39] Z.B. Lei, Z. Liu, H. Wang, X. Sun, L. Lu, X.S. Zhao, J. Mater. Chem. A 1 (2013) 2313.
[40] L.Y. Niu, Z.P. Li, W. Hong, J.F. Sun, Z.F. Wang, L.M. Ma, J.Q. Wang, S.R. Yang, Electrochim. Acta 108 (2013) 666.
[41] Z. Algharaibeh, P.G. Pickup, Electrochem. Commun. 13 (2011) 147.
[42] C.T. Hsu, C.C. Hu, J. Power Sources 242 (2013) 662.
[43] R. Ding, L. Qia, M. Jia, H. Wang, Electrochim. Acta 107 (2013) 494.
[44] C. Tang, Z. Tang, H. Gong, J. Electrochem. Soc. 159 (2012) A651.
[45] X. Wang, A. Sumboja, M.F. Lin, J. Yan, P.S. Lee, Nanoscale 4 (2012) 7266.
[46] X. Wang, W.S. Liu, X.H. Lu, P.S. Lee, J. Mater. Chem. 22 (2012) 23114.
[47] L.Y. Niu, Z. Li, Y. Xu, J. Sun, W. Hong, X. Liu, J. Wang, S. Yang, ACS Appl. Mater. Interfaces 5 (2013) 8044.
[48] B. Senthilkumar, D. Meyrick, Y.S. Lee, R.K. Selvan, RSC Adv. 3 (2013) 16542.
[49] M.C. Liu, L.B. Kong, C. Lu, X.J. Ma, X.M. Li, Y.C. Luo, L. Kang, J. Mater. Chem. A 1 (2013) 1380.